



**UNIVERSITY OF LEEDS**

This is a repository copy of *Anaerobic nitrogen cycling on a Neoproterozoic ocean margin*.

White Rose Research Online URL for this paper:

<http://eprints.whiterose.ac.uk/150242/>

Version: Accepted Version

---

**Article:**

Mettam, C, Zerkle, AL, Claire, MW et al. (3 more authors) (2019) Anaerobic nitrogen cycling on a Neoproterozoic ocean margin. *Earth and Planetary Science Letters*, 527. ARTN: 115800. ISSN 0012-821X

<https://doi.org/10.1016/j.epsl.2019.115800>

---

© 2019 Elsevier B.V. Licensed under the Creative Commons Attribution-NonCommercial-NoDerivatives 4.0 International License (<http://creativecommons.org/licenses/by-nc-nd/4.0/>).

**Reuse**

This article is distributed under the terms of the Creative Commons Attribution-NonCommercial-NoDerivatives (CC BY-NC-ND) licence. This licence only allows you to download this work and share it with others as long as you credit the authors, but you can't change the article in any way or use it commercially. More information and the full terms of the licence here: <https://creativecommons.org/licenses/>

**Takedown**

If you consider content in White Rose Research Online to be in breach of UK law, please notify us by emailing [eprints@whiterose.ac.uk](mailto:eprints@whiterose.ac.uk) including the URL of the record and the reason for the withdrawal request.



[eprints@whiterose.ac.uk](mailto:eprints@whiterose.ac.uk)  
<https://eprints.whiterose.ac.uk/>

1 **Anaerobic nitrogen cycling on a Neoproterozoic ocean margin**

2 **Mettam, C.<sup>a,b,\*</sup>, Zerkle, A.L.<sup>a</sup>, Claire, M.W.<sup>a</sup>, Prave, A.R.<sup>a</sup>, Poulton, S.W.<sup>c</sup>, Junium, C.K.<sup>d</sup>**

3

4 <sup>a</sup> **School of Earth & Environmental Sciences, University of St Andrews, Irvine Building, St Andrews,**  
5 **Fife, KY16 9AL, United Kingdom.**

6 <sup>b</sup> **Department of Earth Sciences, University College London, 5 Gower Place, London, WC1E 6BS,**  
7 **United Kingdom (current address).**

8 <sup>c</sup> **School of Earth and Environment, University of Leeds, Leeds LS2 9JT, United Kingdom.**

9 <sup>d</sup> **Department of Earth Science, Syracuse University, NY 13244-1070, USA.**

10 **\* Corresponding author**

11

12 **Abstract**

13 A persistently aerobic marine nitrogen cycle featuring the biologically mediated oxidation of  
14 ammonium to nitrate has likely been in place since the Great Oxidation Event (GOE) some 2.3 billion  
15 years ago. Although nitrogen isotope data from some Neoproterozoic sediments suggests transient  
16 nitrate availability prior to the GOE, these data are open to other interpretations. This is especially so  
17 as these data come from deep-water environments that were spatially divorced from shallow-water  
18 settings that were the most likely sites for the accumulation of oxygen and the generation of nitrate.  
19 Here we present the first nitrogen isotope data from contemporaneous shallow-water sediments to  
20 constrain the nitrogen cycle in shallow Late Archean settings. The BH-1 Sacha core through the  
21 Campbellrand-Malmani carbonate platform records a transition from a shallow  
22 siliciclastic/carbonate ramp to a rimmed carbonate shelf with the potential for reduced  
23 communication with the open ocean. In these settings nitrogen isotope ( $\delta^{15}\text{N}$ ) data from sub- to

24 peri-tidal and lagoonal settings are close to 0‰, indicating diazotrophy or the complete utilization of  
25 remineralised ammonium with an isotopic composition of near 0‰. Our dataset also includes  
26 negative  $\delta^{15}\text{N}$  values that suggest the presence of an ammonium pool of concentrations sufficient to  
27 have allowed for non-quantitative assimilation. We suggest that this condition may have been the  
28 result of upwelling of phosphorus-rich deep waters into the photic zone, stimulating primary  
29 productivity and creating an enhanced flux of organic matter that was subsequently remineralised  
30 and persisted in the dominantly anoxic Neoproterozoic marine environment. Notably, we find only  
31 limited evidence of coupled nitrification/denitrification, even in these shallow water environments,  
32 calling into question previous suggestions that the Late Archean nitrogen cycle was characterized by  
33 widespread aerobic nitrogen cycling. Rather, aerobic nitrogen cycling was likely spatially  
34 heterogeneous and tied to loci of high oxygen production while zones of shallow water anoxia  
35 persisted.

36

37 Keywords

- 38 • Nitrogen Isotopes
- 39 • Carbon Isotopes
- 40 • Neoproterozoic

41

42

43

44

45

46

47 **1. Introduction**

48 Nitrogen (N) is an essential nutrient for the construction of all biomolecules. Despite the biological  
49 importance of  $N_2$  and its abundance in the atmosphere, only diazotrophic ( $N_2$ -fixing) microbes can  
50 directly assimilate di-nitrogen into biomass, which ultimately provides the primary source of  
51 nitrogen to the biosphere. In the absence of oxygen, the uptake of ammonium ( $NH_4^+$ ) from  
52 remineralised diazotrophic biomass is the primary source of nitrogen for non-diazotrophs. In oxygen-  
53 rich waters,  $NH_4^+$  is rapidly recycled or oxidised by nitrifying microbes to nitrite ( $NO_2^-$ ) and nitrate  
54 ( $NO_3^-$ ). Nitrate is an important component of dissolved inorganic nitrogen (DIN) in oxygenated  
55 waters, and serves as the dominant nitrogen source for primary productivity in modern surface  
56 oceans. In such conditions diazotrophic activity will be reduced due to competition with nitrate  
57 assimilators for other nutrients (e.g. Sigman et al., 2009).

58 In low-oxygen settings, such as modern oxygen minimum zones (OMZs),  $NO_2^-$  and  $NO_3^-$  can also be  
59 utilised as electron acceptors in chemotrophic metabolisms. For example,  $NO_3^-$  can be used in  
60 heterotrophic denitrification or during dissimilatory nitrate reduction to ammonium (DNRA)  
61 (Granger et al., 2008), whilst  $NO_2^-$  is utilised in the anaerobic oxidation of ammonium (anammox).  
62 Importantly, both anammox and denitrification remove bioavailable nitrogen from the oceanic  
63 reservoir and return it to the atmosphere (Cline and Kaplan, 1975), which in extreme cases can lead  
64 to nitrate limitation. When bioavailable nitrogen is scarce an expansion of diazotrophy can occur due  
65 to reduced competition for nutrients, if other nutrients like Fe or bioactive trace elements are not  
66 limiting (Weber and Deutsch, 2013; Sigman et al., 2009).

67 Due to the redox sensitive nature of these N cycling processes, the global N cycle is believed to have  
68 evolved over geologic time alongside changes in the redox state of Earth's oceans and atmosphere  
69 (e.g., Stüeken et al., 2016). The 2.33 Ga Great Oxidation Event (GOE) (Luo et al., 2016) marked the  
70 time when atmospheric oxygen ( $O_2$ ) first exceeded  $10^{-5}$  times present atmospheric levels (PAL), as  
71 constrained by the disappearance of mass-independent fractionation (MIF) of sulphur isotopes

72 (Farquhar et al., 2011; Pavlov and Kasting, 2002). This change in surface redox conditions seemingly  
73 coincided with the widespread expansion of aerobic nitrogen cycling in the world's oceans (e.g.,  
74 Zerkle et al., 2017; Luo et al., 2018). However, this narrative could be overly simplistic. In particular,  
75 small increases of around 2‰ in  $\delta^{15}\text{N}$  values are preserved in the 2.7-2.5 Ga sediments of the  
76 Campbellrand-Malmani carbonate platform from South Africa (Godfrey and Falkowski, 2009), a  
77 setting that is spatially and temporally correlated to the sediments analysed in this study, albeit  
78 further offshore and a deeper depositional setting. Other positive excursions in  $\delta^{15}\text{N}$  are reported  
79 from studies of Australian Neoproterozoic sediments (Garvin et al., 2009; Busigny et al., 2013) and in  
80 all settings these nitrogen isotope values have been explained by transient or localized aerobic  
81 nitrogen cycling. Alternatively, these small positive shifts in  $\delta^{15}\text{N}$  values could represent uptake of a  
82 residual pool of  $^{15}\text{N}$ -enriched ammonium produced by partial nitrification or partial assimilation, or  
83 by nitrogen redox cycling independent of environmental oxygenation (e.g., Thomazo et al., 2011;  
84 Busigny et al., 2013; Ader et al., 2016). However, there are currently no  $\delta^{15}\text{N}$  records of  
85 contemporaneous shallow-water sediments available to distinguish between these alternatives.

86 Here, we investigate  $\delta^{15}\text{N}$  values preserved in shallow-water sediments from the 2.7-2.5 Ga  
87 Campbellrand-Malmani carbonate platform. These sediments, from the BH-1 Sacha core, represent  
88 the shallow-water equivalent to previously investigated deeper-water sediments (GKP01 core;  
89 Fischer et al., 2009), in which  $\delta^{15}\text{N}$  values rose by about 2‰ and were interpreted to represent  
90 transient aerobic nitrogen cycling (Godfrey and Falkowski, 2009). If aerobic nitrogen cycling was  
91 even intermittently pervasive in this basin, we would expect sediments from these shallower water  
92 settings to record similar  $\delta^{15}\text{N}$  values to deeper-water sediments, particularly given their potential  
93 proximity to surface ocean oxygen oases, as shown by the presence of microbial sedimentary  
94 structures (Altermann and Siegfried, 1997).

95

96

## 97 2. Tracking the nitrogen cycle through time

98 Transformations in the marine nitrogen cycle can modify nitrogen isotope signals ( $^{15}\text{N}/^{14}\text{N}$ ;  $\delta^{15}\text{N}$  (‰))  
99 =  $((^{15}\text{N}/^{14}\text{N})_{\text{sample}} / (^{15}\text{N}/^{14}\text{N})_{\text{air}} - 1) \times 1000$ ), leading to fractionation effects between the reactants and  
100 products (Casciotti, 2009; Sigman et al., 2009; Zerkle et al., 2008; Brunner et al., 2013; Möbius, 2013;  
101 Zhang et al., 2014; McCready et al., 1983; Ader et al., 2016). However, in modern settings, most  
102 nitrogen assimilation or redox transformations utilise all available substrates, leading to no apparent  
103 fractionation effects (Sigman et al., 2009). The exceptions are diazotrophy and nitrate/nitrite-  
104 reduction processes, including denitrification, DNRA, and anammox. Diazotrophy generally produces  
105 biomass with  $\delta^{15}\text{N}$  values between  $\sim+1$  and  $\sim-1$ ‰ (Zhang et al., 2014; Bauersachs et al., 2009),  
106 although extreme values as low as  $\sim-4$ ‰ have been experimentally demonstrated (e.g., as reviewed  
107 in Zerkle et al., 2008). The contribution of diazotrophy to total biomass in modern ocean settings is  
108 limited except under oligotrophic conditions, as  $\text{NO}_3^-$  and  $\text{NH}_4^+$  assimilators compete more  
109 successfully for other nutrients (Weber and Deutsch, 2013). However, in most oxygen-rich settings,  
110  $\text{NH}_4^+$  sourced from remineralised biomass is rapidly oxidized, such that nitrate is the main form of  
111 nutrient N. In the modern ocean incomplete denitrification in the water column renders this pool of  
112 bioavailable  $^{15}\text{N}$ -enriched, leading to marine organic matter (OM) with an average  $\delta^{15}\text{N}$  of  $+5$  ‰ to  
113  $+6$ ‰ (Peters et al., 1978; Sigman et al., 2003; Galbraith et al., 2013).

114 The  $\delta^{15}\text{N}$  of marine biomass thus records the dominant forms of bioavailable nitrogen utilised for  
115 primary productivity, particularly on a local scale. These signals are ultimately archived in  
116 sedimentary rocks, either directly in OM or retained as mineral-associated nitrogen derived from  
117 degraded OM (e.g., Stüeken et al., 2016; Freudenthal et al., 1999). Variations in the  $\delta^{15}\text{N}$  of  
118 sedimentary rocks can thus be utilized to track changes in the marine nitrogen cycle through  
119 geological time.

## 120 3. Geological setting

121 The Campbellrand-Malmani Platform in South Africa (Fig. 1A, B and C) is part of the Transvaal  
122 Supergroup. A ~3,700 m section of these rocks was recovered in the BH1-Sacha core and logged in  
123 detail by Altermann and Siegfried (1997). The lowermost recovered strata are a succession of  
124 interbedded doloarenites, quartzites, and shales with microbial laminites from the top of the  
125 Vryburg Formation (Fm) (Altermann and Siegfried, 1997). Thick (> 10 m) shale beds in the lower part  
126 of the core likely represent deeper shelf conditions when marine transgressions mark the beginning  
127 of several deepening and shallowing cycles, with carbonates likely representative of the shallowest  
128 regressive conditions. Thin (< 10 m) shales interbedded with carbonates throughout the core are  
129 mostly likely evidence of slightly deeper lagoonal conditions during generally regressive periods  
130 (Altermann and Siegfried, 1997). A major flooding surface defines the base of the overlying  
131 Boomplaas Fm, but its top is defined by an oolite bed indicating shallow, wave-agitated conditions.  
132 The Lokammona Fm is marked by several, variably developed, shoaling cycles similar to those in the  
133 Vryburg Fm (Sumner and Beukes, 2006). These three formations comprise the Schmidtsdrift  
134 Subgroup, and are overlain by the Monteville Fm of the lowermost Campbellrand Subgroup, which  
135 shows cycles similar to the Lokammona Fm (Sumner and Beukes, 2006). Together, these four  
136 formations are interpreted as representing deposition of sediments on an evolving ramp structure  
137 (Fig. 1B).

138 From the Reivilo Fm upwards, depositional conditions are considered to have been generally  
139 shallow, with subtidal, intertidal or lagoonal conditions dominating as inferred from the presence of  
140 domal, columnar, elongate and small, bifurcating, finger-like stromatolites, birds-eye structures, flat-  
141 pebble breccias and chert beds (Altermann and Siegfried, 1997; Sumner and Beukes, 2006; Fischer  
142 and Knoll, 2009). These facies are considered to represent the replacement of ramp-like conditions  
143 with a rimmed-, carbonate-dominated shallow-shelf, platform-top (Sumner and Grotzinger, 2004;  
144 Sumner and Beukes 2006). A maximum metamorphic grade of sub-greenschist is reported for the  
145 section of the Campbellrand-Malmani Platform studied here (Button, 1973; Miyano and Beukes,  
146 1984; Fischer et al., 2009), consistent with minimal alteration of stable isotope values as indicated by

147 our data (see discussion below). A U-Pb zircon age of  $2,714 \pm 8$  Ma from the underlying Ventersdorp  
148 Supergroup provides a maximum age for the Campbellrand-Malmani Platform (Armstrong et al.,  
149 1991) and tuffs within the Schmidtsdrift and Campbellrand subgroups have yielded stratigraphically  
150 coherent Neoarchaeon ages (Barton et al., 1995; Walraven and Martini, 1995; Fischer et al., 2009;  
151 Knoll and Beukes, 2009; ranges of published dates are in the supplementary material).

#### 152 **4. Methods**

153 Samples were collected from the National Core Repository at Donkerhoek (Pretoria, South Africa).  
154 Sampling was predominantly focussed on black shales, which were anticipated to have high-TOC  
155 content. Samples were ground into homogenous powders in agate ball mills, and carbonate was  
156 removed via two 24 hour digestions in 10 % (vol/vol) HCl. After each digestion the samples were  
157 centrifuged and the supernatant was discarded and replaced with fresh 10% HCl. Sample residues  
158 were washed until pH neutral using ultrapure water ( $18.2 \text{ M}\Omega\cdot\text{cm}$ ) and dried at  $< 40$  °C. Carbonate  
159 content was calculated gravimetrically from dry sample residues which were then homogenised  
160 using an agate pestle and mortar and stored in glass vials. Several samples of mid-grey carbonate  
161 rocks, assumed to contain some OM, were also decarbonated to assess the possibility of extracting  
162 kerogen. This method of carbonate abundance determination is prone to inaccuracy. However, here  
163 it is used only to provide a broad assessment of lithological characteristics, for example between  
164 rocks with high carbonate content (e.g.  $> 85\%$ ), and those with low carbonate concentrations (e.g.  
165  $< 10\%$ ). Kerogen was extracted at the University of St Andrews by digestion of decarbonated residues  
166 in HF/HCl following established protocols (e.g., Zerkle et al., 2017).

167 Nitrogen isotope values for kerogen ( $\delta^{15}\text{N}_{\text{org}}$ ) and decarbonated sediments ( $\delta^{15}\text{N}_{\text{bulk}}$ ) were  
168 determined by nano-EA-IRMS in the GAPP Lab at Syracuse University, USA. Prior to analyses,  
169 samples and standards were placed into a vacuum chamber overnight to remove atmospheric  
170 nitrogen and flooded with Argon (Ar) prior to analysis. Upon introduction into the EA, tin capsule  
171 sealed samples were further purged with helium (He) for 45 seconds prior to combustion in an



172 Elemental Vario Isotope Cube coupled to a Trace Gas analyser. Oxidation and reduction reactor  
173 temperatures were 1100 °C and 650 °C, respectively. Helium carrier gas flow was 150 ml/min; and  
174 the O<sub>2</sub> pulse was set for 90 seconds. Resultant sample gas was trapped in a liquid-N silica gel filled  
175 cryotrap, before release to an Elemental Isoprime 100 IRMS via an Agilent CarboBond capillary  
176 column (25 m x 0.53 mm x 5 um) with a He flow rate of ~2 cm<sup>3</sup> min<sup>-1</sup> (e.g., Polissar et al., 2008; Zerkle  
177 et al., 2017; Luo et al., 2018).

178 Data accuracy for δ<sup>15</sup>N<sub>org</sub> was assessed using the IAEA N1 (Ammonium Sulphate, (NH<sub>4</sub>)<sub>2</sub> SO<sub>4</sub>) standard  
179 which provided a mean δ<sup>15</sup>N value of 0.11± 0.50‰ (1σ; n=30) versus a certified value of +0.40 ±  
180 0.2‰ (1σ).

181 The extremely sensitive nature of the nano-EA-IRMS method generates relatively large peak height  
182 sizes for the blank, in comparison to standard IRMS techniques. This, coupled with relatively  
183 nitrogen-poor kerogen samples, led to blank-sample ratios that could introduce variability in δ<sup>15</sup>N<sub>org</sub>  
184 measurements. Blank-corrected δ<sup>15</sup>N<sub>org</sub> were calculated by blank extraction using the following  
185 equation:

$$186 \quad \delta^{15}\text{N}_{\text{org}} = \frac{(\text{Peak Area}_{\text{sample}} * \delta^{15}\text{N}_{\text{sample}}) - (\text{Peak Area}_{\text{blank}} * \delta^{15}\text{N}_{\text{blank}})}{(\text{Peak Area}_{\text{sample}} - \text{Peak Area}_{\text{blank}})}$$

187 The size (Peak Area<sub>blank</sub>) and isotopic composition of the blank (δ<sup>15</sup>N<sub>blank</sub>) contribution to each  
188 sample measurement was calculated by measuring a blank (without tin cup - as we have found no  
189 difference in blank size and isotopic value whether a tin cup was included or not) before and after  
190 each five samples and calculating incremental change for both values between the two blanks.

191 Duplicates of sample BH1-330, corrected to IAEA N1 indicate reproducibility of δ<sup>15</sup>N<sub>org</sub> was ± 0.02‰  
192 (1σ), whilst triplicates of samples BH1-1963 and BH1-3144.33 produced values ± 0.49‰ (1σ) and ±  
193 0.32‰ (1σ), respectively. Duplicates of samples with large blank contributions resulting from  
194 exceptionally low N<sub>org</sub> produced higher variability, resulting in δ<sup>15</sup>N<sub>org</sub> measurements on samples  
195 below 0.05 wt. % N being discarded. Error bars for δ<sup>15</sup>N<sub>org</sub> plots were calculated using standard

196 deviation of triplicates (BH1-1963.6; 0.49‰) and standard deviation of standards (0.50‰; n=30),  
197 where error bar =  $\sqrt{(\text{error of standards}^2 + \text{largest error of corrected sample}^2)}$ .

198 Decarbonated sediments were also analysed to measure  $\delta^{15}\text{N}_{\text{bulk}}$  values. Again, nitrogen abundances  
199 in these decarbonated residues ( $\text{TN}_{\text{bulk}}$ ) were exceptionally low, ranging from 0.0018 wt. % to 0.017  
200 wt. %, so samples were run in triplicate and  $\delta^{15}\text{N}_{\text{bulk}}$  values determined by Keeling plots. These  
201 samples were corrected to the reference material NIST1547 – Peach Leaves, which returned a  $\delta^{15}\text{N}$   
202 value of +1.76‰ (n=8, determined by Keeling plots) against a certified value of +1.98‰ for  
203 measurement of triplicate samples and +2.10‰ (n=5) for sample 3364 reruns (Table S4). Error bars  
204 for  $\delta^{15}\text{N}_{\text{bulk}}$  reflect the combined standard deviation of standards and the intercept errors of keeling  
205 plots for each individual sample triplicate using the same formula. These individual errors are shown  
206 in supplementary table four.

207 Organic carbon isotope values ( $\delta^{13}\text{C}_{\text{org}}$ ) for this study were measured at the University of St Andrews  
208 via flash-combustion of decarbonated residues using a Costech 4010 EA equipped with a zero blank  
209 autosampler and interfaced with a Thermo Finnigan Delta Plus XP IRMS in continuous flow mode.  
210 Data accuracy was verified using an internal standard (n=5), and returned values of  $-25.07 \pm 0.18\%$   
211 ( $1\sigma$ ) and  $-25.05 \pm 0.11\%$  ( $1\sigma$ ) against an accepted value of  $-25.04\%$ .

212 Nitrogen and carbon isotope values are reported using the standard delta notation showing per mil  
213 deviations from V-PDB for  $\delta^{13}\text{C}$ , and relative to  $\text{N}_{\text{air}}$  for  $\delta^{15}\text{N}$ .

214 The abundance of nitrogen in kerogen ( $\text{N}_{\text{org}}$ ) and in decarbonated residues ( $\text{TN}_{\text{bulk}}$ ) and the total  
215 organic carbon content (TOC) of whole rock powders were calculated by comparing peak areas  
216 generated during isotope analyses with those of standards with known abundances (Table S3 and  
217 S4). To calculate TOC abundances, the carbon yield was adjusted according to the mass lost during  
218 decarbonation.

219 Potassium (K) and iron (Fe) abundances for samples 2709 and 3364 were determined by XRF at  
220 Department of Earth and Environment, Franklin and Marshall College, USA. Standards returned 0.51  
221 wt. %  $\pm 0.0014$  ( $1\sigma$ ) against a certified value of 0.52 wt. % for  $K_2O$  and 12.42 wt. %  $\pm 0.0135$  ( $1\sigma$ )  
222 against a certified value of 12.30 wt. % for  $Fe_2O_3$ . Data for the remaining four samples were analysed  
223 at University of St Andrews using standard XRF providing a standard deviation of  $1\sigma$  of 0.02 wt. % for  
224  $K_2O$ .

## 225 5. Results

226 Nitrogen isotope values from kerogen ( $\delta^{15}N_{org}$ ) for BH1-Sacha (Fig. 2; Table 1) range from  $-2.73\text{‰}$  to  
227  $+3.18\text{‰}$  (mean  $-0.23 \pm 1.59\text{‰}$  here and elsewhere,  $1\sigma$ ,  $n=21$ ). With the exception of samples BH1-  
228 3113.32 and BH1- 3144.33, all  $\delta^{15}N_{org}$  values of greater than  $0\text{‰}$  are from samples with carbonate  
229 abundance in excess of 85% (Fig. 2; Table S1). Bulk nitrogen isotope values ( $\delta^{15}N_{bulk}$ ) range from  $-$   
230  $3.30\text{‰}$  to  $+2.94\text{‰}$  (mean  $+0.58 \pm 2.14\text{‰}$ ,  $n=6$ ). Organic carbon isotope values ( $\delta^{13}C_{org}$ ) for BH1-Sacha  
231 (Fig. 2; Table S1, including a subset from Izon et al. [2015]) range from  $-46.09\text{‰}$  to  $-27.36\text{‰}$  (mean  
232  $-36.69 \pm 3.76\text{‰}$ ,  $n=26$ ).

233 For data binned by depositional setting, the ramp-top settings of the Schmidsdraft Subgroup and  
234 overlying Monteville Fm have mean  $\delta^{15}N_{bulk}$  values of  $+0.11 \pm 2.01\text{‰}$  ( $n=5$ ) and  $\delta^{15}N_{org}$  values of  
235  $+0.22 \pm 1.96\text{‰}$ ,  $n=7$  (Fig. 2; Table S1). The highest  $\delta^{15}N_{org}$  values measured are from two carbonate-  
236 rich facies:  $+2.48\text{‰}$  at 3306.3 m core depth, and  $+3.18\text{‰}$  at 3114.5 m. The highest and lowest  $\delta^{15}N_{org}$   
237 values from siliciclastic facies in this section are  $+0.53\text{‰}$  and  $-2.03\text{‰}$ , whilst  $\delta^{15}N_{bulk}$  values range  
238 from  $-3.30\text{‰}$  to  $+2.02\text{‰}$ . Mean  $\delta^{13}C_{org}$  values from these ramp depositional settings are  $-34.27 \pm$   
239  $3.63\text{‰}$ ,  $n=11$ .

240 In the platform- top/ rimmed-shelf facies from the base of the Reivilo Fm through the Gamohaam  
241 Fm, the mean  $\delta^{15}N_{org}$  values are  $-0.52 \pm 1.36\text{‰}$  ( $n=15$ ) with a single  $\delta^{15}N_{bulk}$  value of  $+2.94\text{‰}$  (Fig. 2;  
242 Table S1). Again, the three carbonate samples had significantly higher  $\delta^{15}N$  values, up to  $+3.17\text{‰}$ .  
243 Mean  $\delta^{13}C_{org}$  values for these facies are  $-38.13 \pm 3.26\text{‰}$  ( $n=15$ ).

## 244 6. Discussion

### 245 6.1. Preservation of Primary Isotopic Signals

246 Diagenetic and metamorphic processes can produce changes in primary carbon and nitrogen isotope  
247 values, generally driving  $\delta^{13}\text{C}_{\text{org}}$  and  $\delta^{15}\text{N}$  values heavier and/or causing a divergence between bulk  
248 rock and kerogen  $\delta^{15}\text{N}$ . At the sub-greenschist facies conditions of the Campbellrand-Malmani  
249 Platform (Button, 1973; Miyano and Beukes, 1984; Fischer et al., 2009) such effects should be  
250 minimal, and not exceed 1 – 2‰ (Stüeken et al., 2017). However, we examined trends in stable  
251 isotope values alongside elemental abundances to evaluate possible contributions from post-  
252 depositional alteration.

253 Thermal maturation during diagenetic or metamorphic processes can preferentially remove  $^{12}\text{C}$  and  
254  $^{14}\text{N}$  from sediments, leading to diagnostic positive correlations between  $\delta^{15}\text{N}_{\text{bulk}}$  and  $\delta^{13}\text{C}_{\text{org}}$ , and  
255 negative correlations between the abundances of TOC and  $\delta^{13}\text{C}_{\text{org}}$ , the abundances of  $\text{TN}_{\text{org}}$  and  
256  $\delta^{15}\text{N}_{\text{org}}$ , and the abundances of  $\text{TN}_{\text{bulk}}$  and  $\delta^{15}\text{N}_{\text{bulk}}$ . We note a weak positive correlation between  $\text{TN}_{\text{org}}$   
257 and  $\delta^{15}\text{N}_{\text{org}}$  ( $R^2 = 0.28$ ; Fig. 3A) and a moderately positive correlation between  $\text{TN}_{\text{bulk}}$  and  $\delta^{15}\text{N}_{\text{bulk}}$  ( $R^2 =$   
258  $0.51$ ; Fig. 3E). We also note a weak positive correlation between  $\delta^{15}\text{N}_{\text{org}}$  and  $\delta^{13}\text{C}_{\text{org}}$  ( $R^2 = 0.24$ ; Fig.  
259 3B) and a weak negative correlation between  $\text{TOC}/\text{TN}_{\text{org}}$  and  $\delta^{15}\text{N}_{\text{org}}$  ( $R^2 = 0.37$ , Fig. 3C). We note no  
260 correlation between TOC and  $\delta^{13}\text{C}_{\text{org}}$  ( $R^2 = 0.10$ ; Fig. 3D), and no correlation between  $\delta^{15}\text{N}_{\text{bulk}}$  and  
261  $\delta^{13}\text{C}_{\text{org}}$  ( $R^2 = 0.05$ ; Fig. 3F). Therefore, our data show little evidence for significant post-depositional  
262 alteration of  $\delta^{13}\text{C}_{\text{org}}$  or  $\delta^{15}\text{N}$ , consistent with the low metamorphic grade of these sediments. We also  
263 examine the potential influence of nitrogen adsorbed onto detrital clays by comparing potassium (K)  
264 content with  $\text{TN}_{\text{bulk}}$  and  $\delta^{15}\text{N}_{\text{bulk}}$  (Figs. 3G and H).

265 We do note that there is a moderate correlation ( $R^2 = 0.69$ ) between K and  $\delta^{15}\text{N}_{\text{bulk}}$  suggesting that  
266 higher concentrations of clay-bound ammonium could be associated with more-positive  $\delta^{15}\text{N}_{\text{bulk}}$   
267 values, although, this correlation is somewhat influenced by the one sample in this small data set.

268 The sample from 3364m is unusual in that negative (-3.3‰)  $\delta^{15}\text{N}_{\text{bulk}}$  values are associated with very  
269 low K abundances (0.97%) in comparison to the remaining samples (Table S6). When this sample is  
270 removed from the analyses the correlation between K and  $\delta^{15}\text{N}_{\text{bulk}}$  is more modest ( $R^2 = 0.32$ ) which  
271 more closely reflects the very limited correlation ( $R^2 = 0.17$ ) between  $\text{TN}_{\text{bulk}}$  and K abundances.

272

## 273 **6.2. Nitrogen cycling in a marginal marine environment**

274 The majority of samples analysed in this study are from relatively thin shale units that were  
275 intercalated with stromatolitic carbonates. These thin shales are interpreted to have been deposited  
276 during small marine transgressions, overprinted upon longer-term, relatively shallow, potentially  
277 lagoonal conditions in platform and ramp-top settings (Altermann and Siegfried, 1997; Sumner and  
278 Beukes, 2006; Ergolu et al., 2017). These thin shales are distinct from thicker shale units that likely  
279 represent more open and deeper marine settings. Given the shallow nature of this setting and the  
280 presence of microbial mats within the photic zone, such conditions should be prime candidates for  
281 pre-GOE oxygen oases. Although the persistence of sulphur MIF in the BH-1 Sacha record indicates  
282 that atmospheric oxygen concentrations must have remained less than 1 ppm during this time (Izon  
283 et al., 2015), oxygen concentrations could have been sufficiently high in the water column or locally  
284 associated with benthic microbial mats to allow for aerobic biogeochemical cycling. Indeed, trace  
285 element and iron speciation analyses from Neoproterozoic sediments of the Campbellrand-Malmani  
286 Platform suggest a stratified ocean with mildly oxygenated surface oxygen oases (Kendall et al.,  
287 2010; Czaja et al., 2012; Eroglu et al., 2015) and localized oxygen production in microbial mats  
288 (Zerkle et al., 2012). Previous studies of trends in  $\delta^{15}\text{N}$  from deeper water sediments from this basin  
289 have also been interpreted to represent transient aerobic N cycling (Godfrey and Falkowski, 2009).

290 We find that  $\delta^{15}\text{N}_{\text{org}}$  values from siliciclastic sediments deposited in these near-shore settings are  
291 inconsistent with widespread coupled nitrification /denitrification. In particular,  $\delta^{15}\text{N}$  values close to

292 ‰ are more consistent with a nitrogen cycle dominated by diazotrophy and the recycling of  $\text{NH}_4^+$ ,  
293 and suggest that any  $\text{NO}_3^-$  generated from localized oxidation of ammonium was quantitatively and  
294 rapidly removed by denitrification and anammox. Even if  $\text{NO}_3^-$  was present, it likely provided a  
295 secondary nutrient N source given that ammonium could have been persistently available under  
296 widely anoxic water column conditions. In modern settings (e.g., Higgins et al., 2012) cyanobacteria  
297 can assimilate both  $\text{NH}_4^+$  and  $\text{NO}_3^-$  as a source of nitrogen, and it has been noted that genes  
298 controlling the assimilation of oxidised nitrogen sources can be repressed in the presence of  
299 ammonium (Flores et al., 2005).

300 The lower part of the BH1-Sacha core (e.g., the Schmidtdrift Subgroup and Monteville Fm)  
301 represents depositional conditions that were likely open to the ocean. Both  $\delta^{15}\text{N}_{\text{bulk}}$  and  $\delta^{15}\text{N}_{\text{org}}$   
302 values in these ramp facies (with the exception of samples at 3114.5m and 3306.3m, discussed  
303 below) are again consistent with anaerobic nitrogen cycling. Intriguingly, one sample (3364m)  
304 provided a  $\delta^{15}\text{N}_{\text{bulk}}$  value of  $-3.3\text{‰}$ , and another sample (3125.05m) a  $\delta^{15}\text{N}_{\text{org}}$  value of  $-2.0\text{‰}$ ,  
305 showing greater  $^{15}\text{N}$  depletion than biomass generally produced by modern marine diazotrophs. This  
306 is especially the case when considering that the long-term diagenetic or metamorphic effects could  
307 possibly have elevated  $\delta^{15}\text{N}$  by a few per mille in comparison to the  $\delta^{15}\text{N}$  of primary organic matter.  
308 We suggest that these strongly negative  $\delta^{15}\text{N}$  values indicate the generation of biomass from partial  
309 assimilation of  $\text{NH}_4^+$ , as recently suggested for  $\sim 2.7$  Ga sediments (Yang et al., 2019). Ammonium  
310 could have accumulated in deep waters under upwelling zones that supported high rates of  
311 diazotrophic productivity and organic matter export (Fig. 4A, B). The remineralisation of this organic  
312 matter at depth under anoxic conditions could have led to the formation of a deep-water  $\text{NH}_4^+$  pool.  
313 In turn, these ammonium-rich waters could have been upwelled, leading to partial  $\text{NH}_4^+$  assimilation  
314 by primary producers, thus forming  $^{15}\text{N}$ -depleted organic matter. Such settings could have included  
315 the ramp front during early platform formation (e.g., thicker shale units at 3364m) and later the  
316 mature platform front (the latter a depositional setting not recorded in the BH1-Sacha core), both of  
317 which represented relatively deeper conditions in contrast to shallow lagoonal depositional settings.

318 Other negative  $\delta^{15}\text{N}$  values (e.g., those associated with thin shales intercalated with carbonates)  
319 could represent times when communication between the lagoonal setting and the open ocean was  
320 more vigorous and allowed  $\text{NH}_4^+$ -rich deep waters to temporarily inundate the lagoon.

321 Sediments at 3364m have high Fe concentrations (14.8%; Table S6) that approach the lower  
322 boundary of Fe abundances in banded iron formations, despite being deposited in open-ramp  
323 conditions. It is possible that in these Fe-rich conditions, diazotrophs utilizing the FeMo nitrogenase  
324 enzyme produced biomass with  $\delta^{15}\text{N}$  values down to -4‰, similar to those reported in Zerkle et al.  
325 (2008). In addition, diazotrophs using alternative nitrogenase enzymes (e.g., Fe-Fe or Fe-V) have  
326 been shown to produced biomass with  $\delta^{15}\text{N}$  values down to -7‰ when Mo is limited (Zhang et al.,  
327 2014). However, large variations in  $\delta^{98}\text{Mo}$  have been reported for the lower Campbellrand-Malmani  
328 Platform, which provide evidence for a sizeable Mo reservoir (Eroglu et al., 2015). It is therefore  
329 unlikely that diazotrophs would have relied on these less efficient alternative enzymes in this  
330 environment.

331 Such low  $\delta^{15}\text{N}$  values are unusual, but not unreported in modern oceans and in the more recent  
332 geologic past (e.g. Higgins et al., 2012). For example,  $\delta^{15}\text{N}$  values of  $\sim -5\text{‰}$  have been reported for  
333 particulate nitrogen, and attributed to the partial utilization of ammonium (Rau et al., 1991) and  
334 nitrate (Altabet and Francois, 1994). In the latter case, these low values are associated with  
335 incomplete utilisation of nitrate in seasonally upwelling waters. However, this degree of  $^{15}\text{N}$ -  
336 depletion is not recorded in subsequent sedimentary  $\delta^{15}\text{N}$  values due to the integration of multiple  
337 seasonal signals representing different rates of nitrate utilisation. The fact that some low  $\delta^{15}\text{N}$   
338 values are recorded in the Neoarchaeon sediments studied here suggests that ammonium had  
339 accumulated to significant levels to remain under-utilised and that nitrogen limitation was not a  
340 significant factor in the wider oceans.

341 Intriguingly, widespread partial assimilation of ammonium could have left the residual pool of  $\text{NH}_4^+$   
342 relatively  $^{15}\text{N}$ -enriched (e.g., Yang et al., 2019). If transported offshore, uptake from a pool of heavier

343  $\text{NH}_4^+$  could generate  $^{15}\text{N}$ -enriched organic matter in more distal ocean settings (Fig. 4A, B; e.g.,  
344 Busigny et al., 2013). This was illustrated numerically by Yang et al. (2019) using a simple Rayleigh  
345 model based on the experimental calibrations of isotope effects during ammonium uptake (Hoch et  
346 al., 1992). This scenario provides an alternative explanation for the presence of positive  $\delta^{15}\text{N}$  values  
347 recorded in relatively distal Neoproterozoic settings in the Gribshunden West Basin (e.g., Godfrey and  
348 Falkowski, 2009).

349 The majority of our  $\delta^{15}\text{N}$  data point to a largely anaerobic marine N cycle, driven by  $\text{N}_2$  fixation and  
350 varying degrees of ammonium uptake and recycling. However, a handful of carbonate-rich facies  
351 show positive  $\delta^{15}\text{N}_{\text{org}}$  values outside the range of typical values for  $\text{N}_2$  fixation (up to +3.2‰; Fig. 4,  
352 Table S1). Elevated  $\delta^{15}\text{N}$  values could indicate syn-depositional oxidative degradation (Freudenthal et  
353 al., 2001; Möbius et al., 2010). However, these  $\delta^{15}\text{N}_{\text{org}}$  values could hint at the potential influence of  
354 nitrification and incomplete denitrification in localised, mildly-oxygenated settings during the  
355 deposition of carbonates, potentially periods when waters were likely shallower than when thin  
356 muds were deposited. Ergolu et al. (2017) have argued that large differences in  $\delta^{13}\text{C}_{\text{org}}$  values  
357 between carbonates and mudstones in the shallower parts of the Campbellrand-Malmani Platform  
358 were due to different consortia of microbes that comprise microbial mats in the two settings. They  
359 suggested that during the deposition of carbonates, microbial mats could have had larger  
360 proportions of oxygenic photoautotroph than during the deposition of mudrocks, with anaerobic  
361 microbes more prevalent during the deposition of the latter. This scenario could support shallow  
362 microbial mat communities as epicentres of highly localised nitrification-denitrification, without a  
363 major role for aerobic N cycling in the Late Archean.

## 364 **6. Conclusions**

365 Here we describe the Neoproterozoic nitrogen cycle in a shallow marginal marine setting, during the  
366 evolution of a well-defined carbonate platform into a relatively isolated platform- top/ rimmed-shelf  
367 lagoonal environment. Nitrogen isotope values range from -3.3 to +3.2‰ and are consistent with a



368 predominantly anaerobic nitrogen cycle, dominated by N<sub>2</sub> fixation and the assimilation and recycling  
369 of upwelling NH<sub>4</sub><sup>+</sup>. Evidence for the presence of oxidised nitrogen species is limited, suggesting that  
370 any NO<sub>3</sub><sup>-</sup> generated during periods of transient oxygen availability was quantitatively removed by  
371 anaerobic respiration. However, rare δ<sup>15</sup>N values > 0 ‰ recorded in carbonate-rich sediments hint at  
372 highly localized areas of nitrification and partial denitrification. In addition, the inclusion of some  
373 very light δ<sup>15</sup>N values suggest partial assimilation of an upwelling pool of ammonium, leaving a  
374 residual pool of <sup>15</sup>N-enriched NH<sub>4</sub><sup>+</sup> that could potentially explain small increases in δ<sup>15</sup>N from  
375 contemporaneous open-ocean settings. We thus conclude that N cycling in the shore-proximal  
376 marine environment of the Griqualand West basin was controlled by anaerobic processes and  
377 recycling of bioavailable nitrogen, and that nitrification/denitrification was unlikely to have been  
378 widespread prior to the end of the Neoproterozoic.

379

### 380 **Acknowledgements**

381 This study was supported financially by NERC Fellowship NE/H016805/2 (to AZ), NERC Standard Grant  
382 NE/J023485/2 (to AZ and MC), NSF EAR-1455258 (to CKJ).

383 We would like to thank the anonymous reviewers for their careful and detailed comments.

384

385

### 386 **References**

387 Ader, M., Thomazo, C., Sansjofre, P., Busigny, V., Papineau, D., Laffont, R., Cartigny, P., Halverson,  
388 G.P., 2016. Interpretation of the nitrogen isotopic composition of Precambrian sedimentary rocks:  
389 Assumptions and perspectives. *Chem. Geol.* 429, 93 - 110.

390

391 Altabet, M.A., 1988. Variations in nitrogen isotopic composition between sinking and suspended  
392 particles: Implications for nitrogen cycling and particle transformation in the open ocean. *Deep Sea*  
393 *Res. A.* 35, 535 – 554.

394

395 Altabet, M.A., Francois, R., 1994. Sedimentary nitrogen isotopic ratio as a recorder for surface ocean  
396 nitrate utilization. *Global biogeochemical cycles* 8, 103 – 116.

397

398 Altermann, W., Siegfried, H.P., 1997. Sedimentology and facies development of an Archaean shelf:  
399 carbonate platform transition in the Kaapvaal Craton, as deduced from a deep borehole at Kathu,  
400 South Africa. *J. Afr. Earth Sci.*, 24, 391 - 410.

401

402 Armstrong, R.A., Compston, W., Retief, E.A., Williams, I.S., Welke, H.J., 1991. Zircon ion microprobe  
403 studies bearing on the age and evolution of the Witwatersrand triad. *Precamb. Res.* 53, 243 - 266.

404

405 Barton, J.M.J., Blignaut, E., Salnikova, E.B., Kotov, A.B., 1995. The stratigraphical position of the  
406 Buffelsfontein Group based on field relationships and chemical and geochronological data. *S. Afr. J.*  
407 *of Geol.* 98, 386 - 392.

408

409 Bauersachs, T., Schouten, S., Compaoré, J., Wollenzien, U., Stal, L.J., Damsteé, J.S.S., 2009. Nitrogen  
410 isotopic fractionation associated with growth on dinitrogen gas and nitrate by cyanobacteria. *Limnol.*  
411 *Oceanogr.* 5, 1403 - 1411.

412

413 Brunner, B., Contreras, S., Lehmann, M.F., Matantseva, O., Rollog, M., Kalvelage, T., Klockgether, G.,  
414 Lavik, G., Jetten, M.S.M., Kartal, B., Kuypers M.M., 2013. Nitrogen isotope effects induced by  
415 anammox bacteria. *P.N.A.S.* 110, 18994 - 18999.

416

417 Busigny, V., Lebeau, O., Ader, M., Krapez, B., Bekker, A., 2013. Nitrogen cycle in the Late Archean  
418 ferruginous ocean. *Chem. Geol.* 362, 115 - 130.

419

420 Button, A., 1973. The stratigraphic history of the Malmani dolomite in the eastern and north-eastern  
421 Transvaal. *Verh. Geol. Ver. S.-Afr.* 76, 229 - 247.

422

423 Casciotti, K.L. 2009. Inverse kinetic isotope fractionation during bacterial nitrite oxidation. *Geochim.*  
424 *Cosmochim. Acta.* 73, 2061 - 2076.

425

426 Cline, J.D., Kaplan I.R., 1975. Isotopic fractionation of dissolved nitrate during denitrification in the  
427 eastern tropical north Pacific Ocean. *Marine Chem.* 3, 271 - 299.

428

429 Czaja, A.D., Johnson, C.M., Roden, E.E., Beard, B.L., Voegelin, A.R., Nägler, T.F., Beukes, N.J., Wille,  
430 M., 2012. Evidence for free oxygen in the Neoproterozoic ocean based on coupled iron–molybdenum  
431 isotope fractionation. *Geochim. Cosmochim. Acta.* 86, 118 - 137.

432

433 Eroglu, S., Schoenberg, R., Wille, M., Beukes, N., Taubald, H., 2015. Geochemical stratigraphy,  
434 sedimentology, and Mo isotope systematics of the ca. 2.58–2.50 Ga-old Transvaal Supergroup  
435 carbonate platform, South Africa. *Precamb. Res.* 266, 27 - 46.

436

437 Eroglu, S. van Zuilen, M.A., Taubald, H., Drost, K., Wille, M., Swanner, E.D., Beukes, N.J., Schoenberg,  
438 R., 2017. Depth-dependent  $\delta^{13}\text{C}$  trends in platform and slope settings of the Campbellrand-Malmani  
439 carbonate platform and possible implications for Early Earth oxygenation. *Precamb. Res.* 302, 122 -  
440 139.

441

442 Farquhar, J., Zerkle, A.L., Bekker, A., 2011. Geological constraints on the origin of oxygenic  
443 photosynthesis. *Photosynth. Res.* 107, 11 - 36.

444

445 Fischer, W.W., Schroeder, S., Lacassie, J.P., Beukes, N.J., Goldberg, T., Strauss, H., Horstmann, U.E.,  
446 Schrag, D.P., Knoll, A.H., 2009. Isotopic constraints on the Late Archean carbon cycle from the  
447 Transvaal Supergroup along the western margin of the Kaapvaal Craton, South Africa. *Precambrian*  
448 *Res.* 169 15 - 27.

449

450 Fischer, W.W., Knoll, A.H., 2009. An iron shuttle for deep water silica in Late Archean and early  
451 Paleoproterozoic iron formation. *G.S.A. Bull.* 121, 222 - 235.

452

453 Flores, E., Frías, J.E., Rubio, L.M., Herrero, A., 2005. Photosynthetic nitrate assimilation in  
454 cyanobacteria. *Photosynth. Res.* 83: 117 – 133.

455

456 Freudenthal, T., Wagner, T., Weinzhöffer, F., Zabel, M., Wefer, G., 2001. Early diagenesis of organic  
457 matter from sediments of the eastern subtropical Atlantic: Evidence from stable nitrogen and carbon  
458 isotopes. *Geochim. Cosmochim. Acta.* 65, 1795 - 1808.

459

460 Galbraith, E.D., Kienast, M., & The NICOPP working group members, 2013. The acceleration of  
461 oceanic denitrification during deglacial warming. *Nat. Geosci.* 6, 579 - 584.

462

463 Garvin, J., Buick, R., Anbar, A.D., Arnold, G.L., Kaufman, A.J., 2002. Isotopic evidence for an aerobic  
464 nitrogen cycle in the latest Archean. *Science.* 323, 1045 - 1048.

465

466 Godfrey, L.V., Falkowski, P.G., 2009. The cycling and redox state of nitrogen in the Archaean ocean.  
467 *Nat. Geosci.* 2, 735 - 729.

468

469 Granger, J., Sigman, D.M., Lehmann, M.F., Tortell P.D., 2008. Nitrogen and oxygen isotope  
470 fractionation during dissimilatory nitrate reduction by denitrifying bacteria. *Limnol. Oceanogr.* 53,  
471 2533 - 2545.

472

473 Higgins, M.B., Robinson, R.S., Husson, J.M., Carter, S.J., Pearson, A., 2012. Dominant eukaryotic  
474 export production during ocean anoxic events reflects the importance of recycled  $\text{NH}_4^+$ . *PNAS.* 109,  
475 2269 - 2274.

476

477 Hoch, M.P., Fogel, M.L., Kirchman, D.L., 1992. Isotope fractionation associated with ammonium  
478 uptake by a marine bacterium. *Limnol. Oceanogr.* 37, 1447 - 1459.

479

480 Izon, G., Zerkle, A.L., Zhelezinskaia, I., Farquhar, J., Newton, R.J., Poulton, S.W., Eigenbrode, J.L.,  
481 Claire, M.W., 2015. Multiple oscillations in Neoproterozoic atmospheric chemistry. *E.P.S.L.* 431, 264 -  
482 273.

483

484 Kendall, B., Reinhard, C.T., Lyons, T.W., Kaufman, A.J., Poulton, S.W., Anbar, A.D., 2010. Pervasive  
485 oxygenation along late Proterozoic ocean margins. *Nat. Geosci.* 3, 647-652.

486

487 Knoll, A.H., Beukes, N.J., 2009. Introduction: Initial investigations of a Neoproterozoic shelf margin-basin  
488 transition (Transvaal Supergroup, South Africa). *Precamb. Res.* 169, 1 - 14.

489

490 Luo, G., Shuhei Ono, S., Nicolas J. Beukes, N.J., David T. Wang, D.T., Shucheng Xie, S., Summons, R.E.  
491 2016. Rapid oxygenation of Earth's atmosphere 2.33 billion years ago. *Science Advances* 13, 2,  
492 e1600134

493

494 Luo, G., Junium, C.K., Izon, G., Ono, S., Beukes, N.J., Algeo, T.J., Cui, Y., Xie, S., Summons, R.E., 2018.  
495 Nitrogen fixation sustained productivity in the wake of the Palaeoproterozoic Great Oxygenation  
496 Event. *Nat. Comms.* 9, 978.

497

498 McCready, R.G.L., Gould, W.D., Barendregt, R.W., 1983. Nitrogen isotope fractionation during the  
499 reduction of  $\text{NO}_3^-$  to  $\text{NH}_4^+$  by *Desulfovibrio* sp. *Canadian Jour. Microbiol.* 29, 231 - 234.  
500

501 Miyano, T., Beukes, N.J., 1984. Phase relations of stilpnomelane, ferri-annite, and riebeckite in very  
502 low grade metamorphosed iron formations. *Verh. Geol. Ver. S.-Afr.* 87, 111 - 124.  
503

504 Möbius, J., Lahajnar, N., Emeis K-C., 2010. Diagenetic control of nitrogen isotope ratios in Holocene  
505 sapropels and recent sediments from the Eastern Mediterranean Sea. *Biogeosci.* 7, 3901 - 3914.  
506

507 Möbius, J., 2013. Isotope fractionation during nitrogen remineralization (ammonification):  
508 implications for nitrogen isotope biogeochemistry. *Geochim. Cosmochim. Acta.* 105, 422-432.  
509

510 Pavlov, A.A., Kasting, J.F., 2002. Mass-independent fractionation of sulfur isotopes in Archean  
511 sediments: strong evidence for an anoxic Archean atmosphere. *Astrobiology.* 2, 27 - 41.  
512

513 Peters, K.E., Sweeney, R.E., Kaplan, I.R., 1978. Correlation of carbon and nitrogen stable isotope  
514 ratios in sedimentary organic matter. *Limn. Ocean.* 23, 598 - 604.  
515

516 Polissar, P.J., Fulton, J.M., Junium, C.K., Courtney C. Turich, C.C., Freeman, K.H., 2009. Measurement  
517 of  $^{13}\text{C}$  and  $^{15}\text{N}$  Isotopic Composition on Nanomolar Quantities of C and N. *Anal. Chem.* 81, 755 - 763.  
518

519 Rau, G.H., Sullivan, W., Gordon, L.I., 1991.  $\delta^{13}\text{C}$  and  $\delta^{15}\text{N}$  variations in Weddell Sea particulate  
520 organic matter. *Marine Chemistry*, 35, 355 – 369.

521

522 Sigman, D. M., Robinson, R., Knapp, A.N., van Geen, A., McCorkle, D. C., Brandes, J.A., Thunell, R.C.,  
523 2003. Distinguishing between water column and sedimentary denitrification in the Santa Barbara  
524 Basin using the stable isotopes of nitrate. *Geochem. Geophys. Geosys.* 4, 1040.

525

526 Sigman, D.M., Karsh, K.L., Casciotti, K.L., 2009. Ocean process tracers: Nitrogen isotopes in the  
527 ocean. In: Steele, J.H., Turekian, K.K., (Eds.) *Encyclopedia of Ocean Sciences*. London: Academic  
528 Press.

529

530 Stüeken, E.E., Kipp, M.A., Koehler, M.C., Buick, R., 2016. The evolution of Earth's biogeochemical  
531 nitrogen cycle. *Earth Sci. Rev.*, 160, 220 - 239.

532

533 Stüeken, E.E., Zaloumis, J., Meixnerová, J., Buick, R., 2017. Differential metamorphic effects on  
534 nitrogen isotopes in kerogen extracts and bulk rocks. *Geochim. Cosmochim. Acta.* 217, 80 - 94.

535

536 Sumner, D.Y., Grotzinger, J.P., 2004. Implications for Neoproterozoic ocean chemistry from primary  
537 carbonate mineralogy of the Campbellrand-Malmani Platform, South Africa. *Sedimentology.* 51,  
538 1273 - 1299.

539



540 Sumner, D.Y., Beukes, N.J., 2006. Sequence stratigraphic development of the Neoproterozoic Transvaal  
541 carbonate platform, Kapvaal Craton, South Africa. *S. Afr. J. Geol.* 109, 11 - 22.

542

543 Thomazo, C., Ader, M., Philippot, P., 2011. Extreme <sup>15</sup>N-enrichments in 2.72-Gyr-old sediments:  
544 evidence for a turning point in the nitrogen cycle. *Geobiology*. 9, 107 - 120.

545

546 Walraven, F. and Martini, J., 1995. Zircon Pb-evaporation age determinations of the  
547 Oak Tree Formation, Chuniesport Group, Transvaal Sequence: Implications for Transvaal-Griqualand  
548 West basin correlations. *S. Afr. J. of Geol.* 98, 58 - 67.

549

550 Walter M., Grotzinger J.P., Schopf J.W., 1992. Proterozoic stromatolites. In: Schopf J.W., Klein C.  
551 (Eds.), *The Proterozoic biosphere. A multidisciplinary study*, Cambridge Univ. Press, Cambridge. 253 -  
552 260.

553

554 Weber, T., Deutsch, C., 2014. Local versus basin-scale limitation of marine nitrogen fixation. *P.N.A.S.*  
555 111, 8741 - 8746.

556

557 Yang, J., C. K. Junium, C.K., Grassineau, N.V., Nisbet, E.G., Izon, G., Mettam, C., Martin, A., Zerkle,  
558 A.L., 2019. Ammonium availability in the Late Archaean nitrogen cycle. *Nat. Geosci.*  
559 <https://doi.org/10.1038/s41561-019-0371-1>

560

561 Zerkle, A.L., Junium, C.K., Canfield, D.E., House, C.H., 2008. Production of <sup>15</sup>N-depleted biomass  
562 during cyanobacterial N<sub>2</sub>-fixation at high Fe concentrations. *Jour. Geophys. Res.* 113,  
563 doi:10.1029/2007JG000651.

564

565 Zerkle, A.L., Claire, M.W., Domagal-Goldman, S.D., Farquhar, J., Poulton, S. W., 2012. A bistable  
566 organic-rich atmosphere on the Neoproterozoic Earth. *Nat. Geosci.* 5, 359 - 363.

567

568 Zerkle, A.L., Poulton, S.W., Newton, R.J., Mettam, C., Claire, M.W., Bekker, A., Junium, C.K., 2017.  
569 Onset of the aerobic nitrogen cycle during the Great Oxidation Event. *Nature.* 542, 465 - 467.

570

571 Zhang, X., Sigman, D.M., Morel, F.M., Kraepiel, A.M., 2014. Nitrogen isotope fractionation by  
572 alternative nitrogenases and past ocean anoxia. *P.N.A.S.* 111, 4782 - 4787.

573

574

575

576

577

578

579

580

581

## 582 Figure Legends

583 **Fig 1.** (A) Simplified stratigraphy of BH1-Sacha core (Altermann and Siegfried, 1997). (B) Simplified  
584 structure of Campbellrand-Malmani platform-top and ramp showing placement of BH1-Sacha core  
585 (Sumner and Beukes, 2006). (C) Position of BH1-Sacha drill site (star symbol) in South Africa (Sumner  
586 and Beukes, 2006). Dates in Figs. A and B are from a review in Sumner and Beukes (2009). More  
587 dates and references from correlative stratigraphy are presented in the supplementary information  
588 which confirm a date of 2588 to 2549 Ma for the Monteville Fm.

589

590 **Fig. 2.** Geochemical data for BH1-Sacha core. Nitrogen isotope data  $\delta^{15}\text{N}_{\text{org}}$  (‰) are shown as black  
591 dots for silicates and triangles for carbonates, whilst  $\delta^{15}\text{N}_{\text{bulk}}$  (‰) are shown as open pentagons).  
592 Carbonate abundance data (wt. %) are shown as dots. TOC (wt. %) and  $\delta^{13}\text{C}_{\text{org}}$  (‰) data from this  
593 study are shown as dots, whilst data from Izon et al. (2015) are shown as open squares. Symbols for  
594 lithologies in core diagram as per Fig. 1A. Error bars for  $\delta^{15}\text{N}_{\text{org}}$  reflect the combined standard  
595 deviation of N1 standards and triplicates of sample BH1-1963.6 using the equation: error bar =  $v$  (

596 **Fig. 3.** Cross plots of geochemical data. Filled circles represent data from this study. Open squares  
597 include TOC and  $\delta^{13}\text{C}_{\text{org}}$  data from Izon et al. (2015). Data shown: (A)  $\text{TN}_{\text{org}}$  and  $\delta^{15}\text{N}_{\text{org}}$ , (B)  $\delta^{15}\text{N}_{\text{org}}$   
598 and  $\delta^{13}\text{C}_{\text{org}}$ , (C)  $\text{TOC}/\text{TN}_{\text{org}}$  and  $\delta^{15}\text{N}_{\text{org}}$  (D) TOC and  $\delta^{13}\text{C}_{\text{org}}$ , (E)  $\text{TN}_{\text{bulk}}$  and  $\delta^{15}\text{N}_{\text{bulk}}$ , (F)  $\delta^{15}\text{N}_{\text{bulk}}$  and  
599  $\delta^{13}\text{C}_{\text{org}}$ , (G) potassium and  $\delta^{15}\text{N}_{\text{bulk}}$  and (H)  $\text{TN}_{\text{bulk}}$  and  $\delta^{15}\text{N}_{\text{bulk}}$ .

600

601 **Fig. 4.** Proposed model for facies-dependent nitrogen cycling at the ocean margin. This depositional  
602 setting is a well-defined marine marginal ramp and platform-top that could have reduced  
603 communication with the open ocean and led to somewhat isolated shallow **depositional settings**.  
604 Platform/ramp bathymetry and stromatolite assemblages are based upon idealised Proterozoic  
605 ramp and platform settings by Walter et al. (1992). Shown here are: **(A)** a shallow ramp top setting,  
606 representing the Schmidtsdrift Subgroup and Monteville Fm; and **(B)** a lagoonal depositional setting,  
607 representing the Campbellrand Subgroup overlying the Monteville Fm. The proposed mechanisms  
608 include: **(1)** transport of diazotrophic biomass to the seafloor; **(2)** remineralization of OM to  $\text{NH}_4^+$   
609 and shoreward transport; **(3)**  $\text{NH}_4^+$  assimilation, producing OM with -ve  $\delta^{15}\text{N}$  values; **(4)** transport of  
610 a residual pool of  $\text{NH}_4^+$  (possibly with +ve  $\delta^{15}\text{N}$  values); **(5)** open ocean ammonium assimilation,  
611 producing OM with +ve  $\delta^{15}\text{N}$  values; and, **(6)** potential for restricted open-marine influence but **(7)**  
612 potential for variability in communication as sea levels fluctuated.

613

614

615

616

617

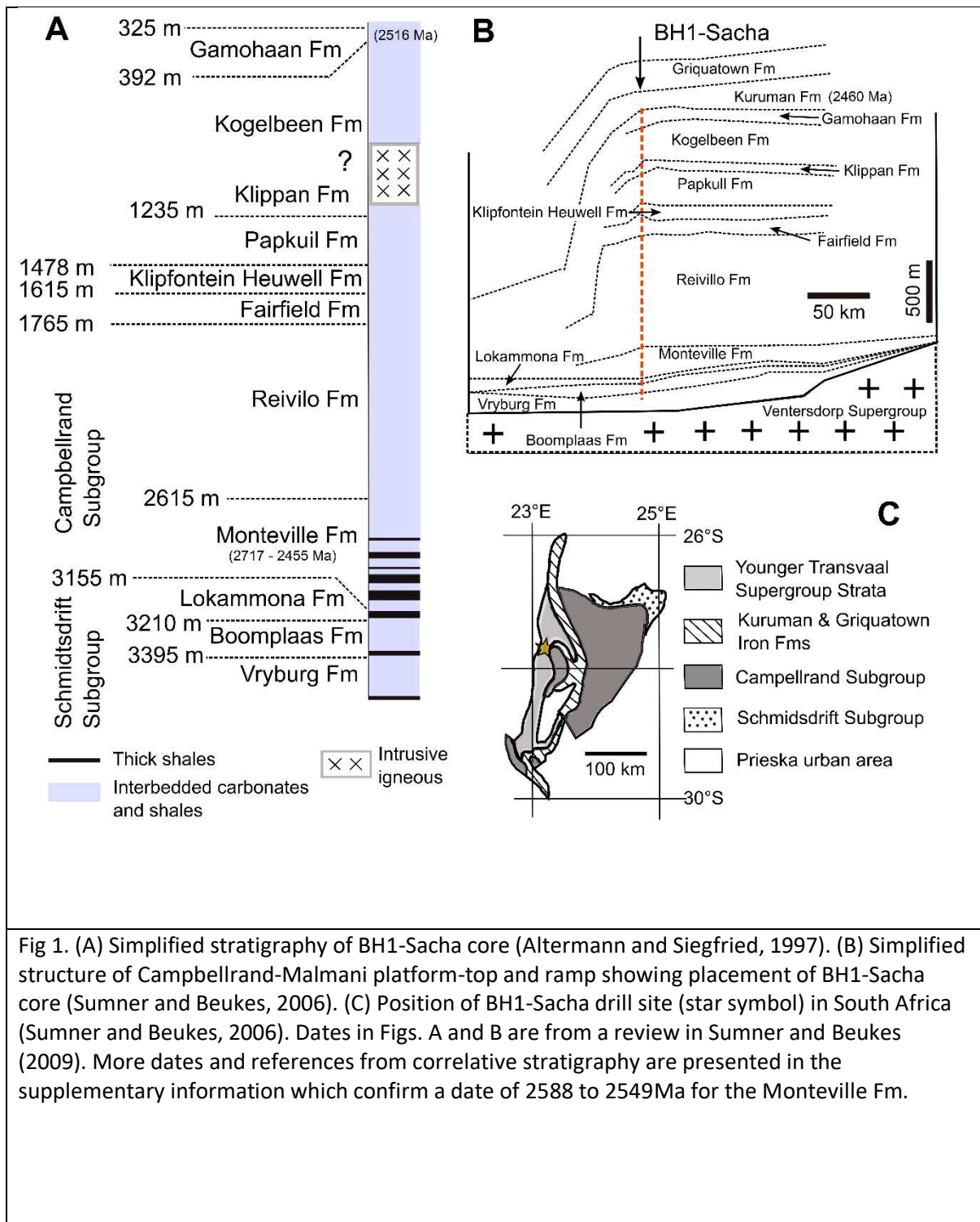


Fig 1. (A) Simplified stratigraphy of BH1-Sacha core (Altermann and Siegfried, 1997). (B) Simplified structure of Campbellrand-Malmani platform-top and ramp showing placement of BH1-Sacha core (Sumner and Beukes, 2006). (C) Position of BH1-Sacha drill site (star symbol) in South Africa (Sumner and Beukes, 2006). Dates in Figs. A and B are from a review in Sumner and Beukes (2009). More dates and references from correlative stratigraphy are presented in the supplementary information which confirm a date of 2588 to 2549Ma for the Monteville Fm.

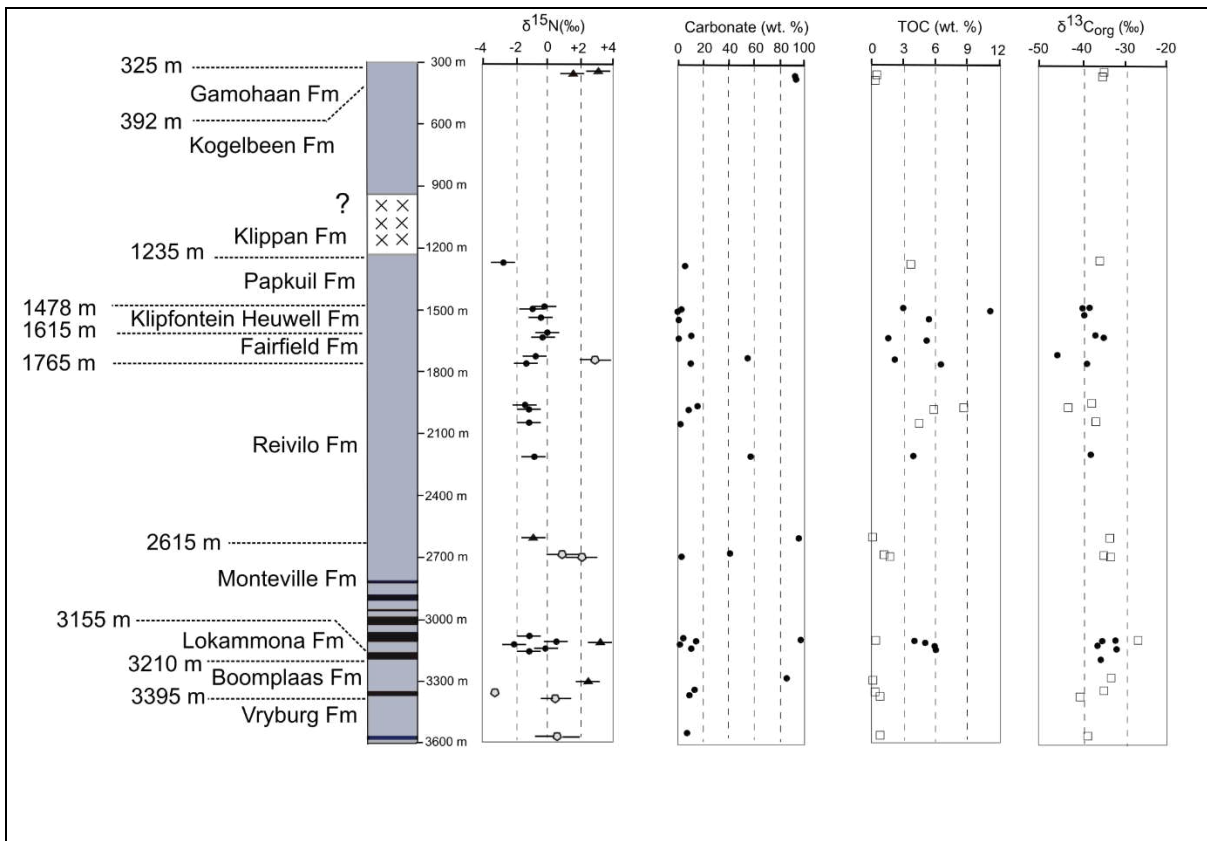


Fig. 2. Geochemical data for BH1-Sacha core. Nitrogen isotope data  $\delta^{15}\text{N}_{\text{org}}$  (‰) are shown as black dots for silicates and triangles for carbonates, whilst  $\delta^{15}\text{N}_{\text{bulk}}$  (‰) are shown as open pentagons). Carbonate abundance data (wt. %) are shown as dots. TOC (wt. %) and  $\delta^{13}\text{C}_{\text{org}}$  (‰) data from this study are shown as dots, whilst data from Izon et al. (2015) are shown as open squares. Symbols for lithologies in core diagram as per Fig. 1A. Error bars for  $\delta^{15}\text{N}_{\text{org}}$  reflect the combined standard deviation of N1 standards and triplicates of sample BH1-1963.6 using the equation: error bar =  $\sqrt{(\text{error of standards}^2 + \text{largest error of corrected sample}^2)}$ . Error bars are thus  $\pm 0.7\text{‰}$ . Error bars for  $\delta^{15}\text{N}_{\text{bulk}}$  reflect the combined standard deviation of standards and the intercept errors of keeling plots for each sample triplicate using the same formula. These are shown in the supplementary tables.

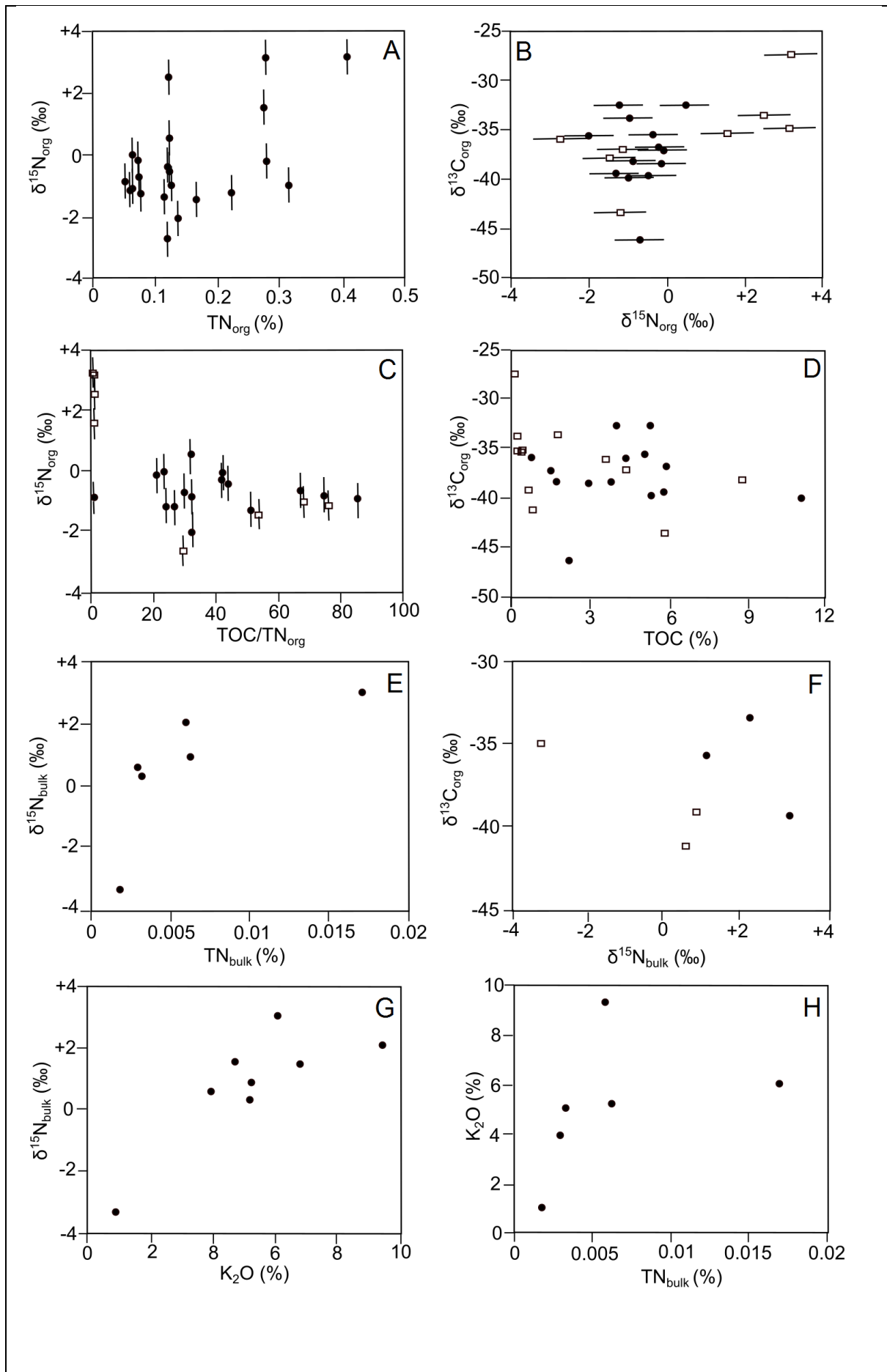
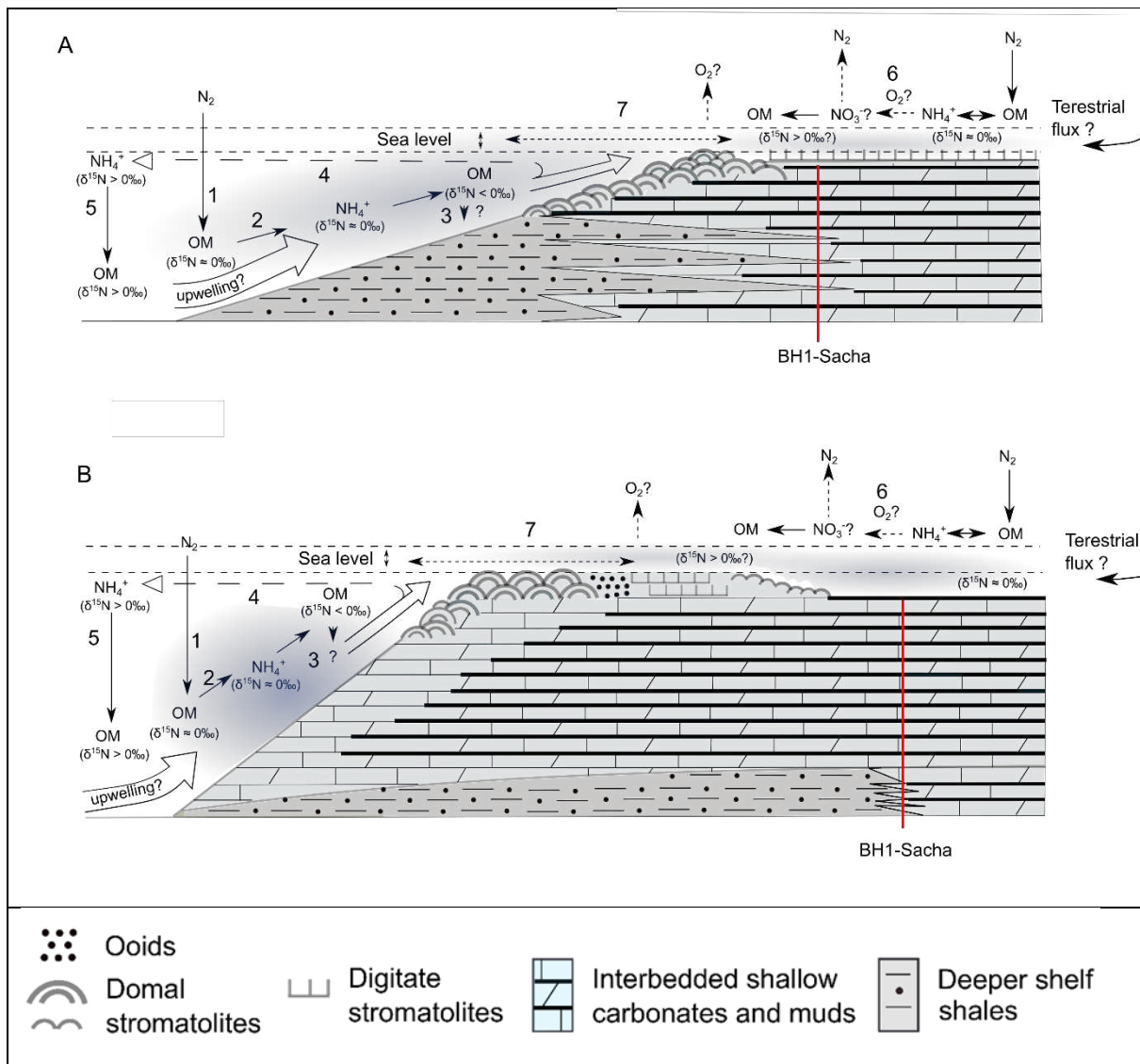


Fig. 3. Cross plots of geochemical data. Filled circles represent data from this study. Open squares include TOC and  $\delta^{13}\text{C}_{\text{org}}$  data from Izon et al. (2015). Data shown: (A)  $\text{TN}_{\text{org}}$  and  $\delta^{15}\text{N}_{\text{org}}$ , (B)  $\delta^{15}\text{N}_{\text{org}}$  and  $\delta^{13}\text{C}_{\text{org}}$ , (C)  $\text{TOC}/\text{TN}_{\text{org}}$  and  $\delta^{15}\text{N}_{\text{org}}$  (D)  $\text{TOC}$  and  $\delta^{13}\text{C}_{\text{org}}$ , (E)  $\text{TN}_{\text{bulk}}$  and  $\delta^{15}\text{N}_{\text{bulk}}$ , (F)  $\delta^{15}\text{N}_{\text{bulk}}$  and  $\delta^{13}\text{C}_{\text{org}}$ , (G) potassium and  $\delta^{15}\text{N}_{\text{bulk}}$  and (H)  $\text{TN}_{\text{bulk}}$  and  $\delta^{15}\text{N}_{\text{bulk}}$ .

623



**Fig. 4.** Proposed model for facies-dependent nitrogen cycling at the ocean margin. This depositional setting is a well-defined marine marginal ramp and platform-top that could have reduced communication with the open ocean and led to somewhat isolated shallow depositional settings. Platform/ramp bathymetry and stromatolite assemblages are based upon idealised Proterozoic ramp and platform settings by Walter et al. (1992). Shown here are: **(A)** a shallow ramp top setting, representing the Schmidrift Subgroup and Monteville Fm; and **(B)** a lagoonal depositional setting, representing the Campbellrand Subgroup overlying the Monteville Fm. The proposed mechanisms include: **(1)** transport of diazotrophic biomass to the seafloor; **(2)** remineralization of OM to  $\text{NH}_4^+$  and shoreward transport; **(3)**  $\text{NH}_4^+$  assimilation, producing OM with -ve  $\delta^{15}\text{N}$  values; **(4)** transport of a residual pool of  $\text{NH}_4^+$  (possibly with +ve  $\delta^{15}\text{N}$  values); **(5)** open ocean ammonium assimilation, producing OM with +ve  $\delta^{15}\text{N}$  values; and, **(6)** potential for

restricted open-marine influence but **(7)** potential for variability in communication as sea levels fluctuated.

624

625

626